Scheme III

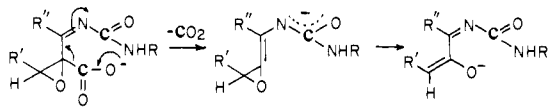

a single acid dissociation constant (pK_a = 3.00, attributable to the carboxyl group) and rate constants for reaction with protonated (HA, k_{1HA} = 0.81 min^{-1}) and ionized (A$^-$, k_{1A^-} = 7.5 × 10^{-2} min^{-1}) forms of intermediate A. Although reaction of the neutral free acid is kinetically indistinguishable from a mechanism involving an oxirane-protonated glycidate salt, results[12] obtained for the decarboxylation of other simpler glycidic acid derivatives argue in favor of a zwitterionic mechanism (eq 1). The value obtained

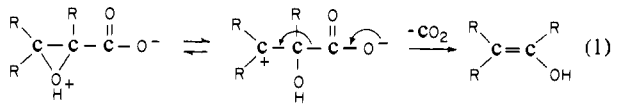

(1)

for k_{1HA} is not very different from that observed for the decarboxylation of 2,3-epoxy-3-phenylbutanoic acid (k = 1.7 min^{-1}).[13] This suggests that the carbamoylimino group β to the carboxyl function in intermediate A has only a small effect on the reaction of the protonated intermediate. Although a slower rate is observed for the ionized intermediate, the latter exhibits enhanced reactivity as compared with the 2,3-epoxy-3-phenylbutanoate anion, where decarboxylation is not detectable.[13] This difference suggests that the β-carbamoylimino group may participate in the reaction with ionized intermediate A, possibly via a mechanism where decarboxylation precedes epoxide ring opening (Scheme III).

Intermediate B (λ_{max} = 346, 357 nm) is observed at pH >12 (Figure 2), where the rate of conversion of the intermediate to compound C (k_2) is slow and rate determining (k_1 = 6.7 × 10^{-2} min^{-1}, k_2 = 2.2 × 10^{-2} min^{-1}, pH 12.2).[14] Since similar values are observed for k_1 at pH 11.1 (6.6 × 10^{-2} min^{-1}) and pH 12.2, the change in the rate-determining step of the reaction in this pH range indicates that the rate of conversion of intermediate B to compound C increases with decreasing pH. This is consistent with the immediate conversion of intermediate B to compound C that is observed at neutral pH. Formation of intermediate B by reaction of compound C with excess methylamine is observed over a wider pH range (pH >10), and an intermediate with similar properties is detected at neutral pH in reactions observed with enzyme-bound epoxide, where the intermediate is subject to kinetic stabilization by the protein moiety. Studies to evaluate parameters affecting the stability of free vs. enzyme-bound intermediate B are in progress.[15]

Acknowledgment. This work was supported by a grant from the National Institutes of Health (GM22662). FT NMR spectra (300 MHz) were obtained at The Ohio State University Chemical Instrument Center (funded in part by National Science Foundation Grant CHE-7910019) with the help of Dr. C. E. Cottrel and Dr. A. G. Marshall.

Registry No. A, 82740-77-0; B, 82740-78-1; C, 80885-76-3; 3,10-dimethyl-5-deazaisoalloxazine 4a,5-epoxide, 72278-21-8; 10-methyl-5-deazaisoalloxazine 4a,5-epoxide, 72283-85-3; methylamine, 74-89-5; 3,10-dimethyl-5-deazaisoalloxazine, 38559-35-2.

(11) Bevington, P. R. "Data Reduction and Error Analysis for the Physical Sciences"; McGraw-Hill: New York, 1969; pp 237–240.
(12) Singh, S. P.; Kagan, J. *J. Org. Chem.* **1970**, *35*, 2203–2207.
(13) Shiner, V. J.; Martin, B. *J. Am. Chem. Soc.* **1962**, *84*, 4824–4827.
(14) (a) On the basis of the observed values for k_1 and k_2, a maximum yield for intermediate B at pH 12.2 can be calculated[14b] (58% at 25 min). The latter value corresponds to the time when absorbance at 375 nm reaches a maximum value. (b) Frost, A. A.; Pearson, R. B. "Kinetics and Mechanism"; Wiley: New York, 1961; p 168.
(15) The pyrimidine ring contraction reaction with 5-deazaflavin 4a,5-epoxide reported in this communication has been confirmed by Yoneda and Sakuma (Yoneda, F.; Sakuma, Y. *Tetrahedron Lett.* **1981**, *22*, 3977–3980) in a paper that appeared after this manuscript was submitted for publication. These workers proposed a different mechanism involving decarboxylation as a final step, which appears inconsistent with our studies, which show that the last step in the reaction is reversible in the presence of excess methylamine.

Resonance Raman Detection of an Fe–S Bond in Cytochrome P450$_{cam}$

P. M. Champion,*† B. R. Stallard,‡ G. C. Wagner,§ and I. C. Gunsalus§

Contribution from the Department of Chemistry, Worcester Polytechnic Institute, Worcester, Massachusetts 01609, the Department of Chemistry, Cornell University, Ithaca, New York 14853, and the Department of Biochemistry, University of Illinois, Urbana, Illinois 61801. *Received December 15, 1981*

Abstract: Resonance Raman scattering experiments on isotopically labeled samples of the oxidized cytochrome P450$_{cam}$–substrate complex conclusively demonstrate the existence of an Fe–S bond that is sensitive to the presence of substrate. A general three-body oscillator model is developed that predicts the observed Raman frequency shifts of the 351-cm^{-1} Fe–S stretching mode due to the isotropic substitution.

We report results of resonance Raman scattering experiments on isotopically enriched (^{54}Fe, ^{34}S) and natural-abundance (^{56}Fe, ^{32}S) samples of the heme protein cytochrome P450$_{cam}$. These experiments provide the first direct and independent evidence of an Fe–S bond in the oxidized enzyme–substrate complex. The observed isotopic shifts of the 351-cm^{-1} Raman-active vibration are quantitated within a general three-body normal-mode oscillator model that is sensitive to the Fe–S–C bond angle. Moreover, the present data, along with previous work on the substrate-free enzyme, indicate that substrate binding produces a significant change in the iron–sulfur interaction.

Cytochrome P450 monoxygenases exhibit a close homology in catalytic and heme active-site parameters, despite a diverse range of xenobiotic detoxification, carcinogenic, and biosynthetic steroid functions.[1] Although the modes of electron transport and sub-

† Worcester Polytechnic Institute
‡ Cornell University.
§ University of Illinois.

(1) Coon, M. J.; White, R. E. In "Dioxygen Binding and Activation by Metal Centers"; Spiro, T. G., Ed.; Wiley: New York, 1980; p 73.

0002-7863/82/1504-5469$01.25/0

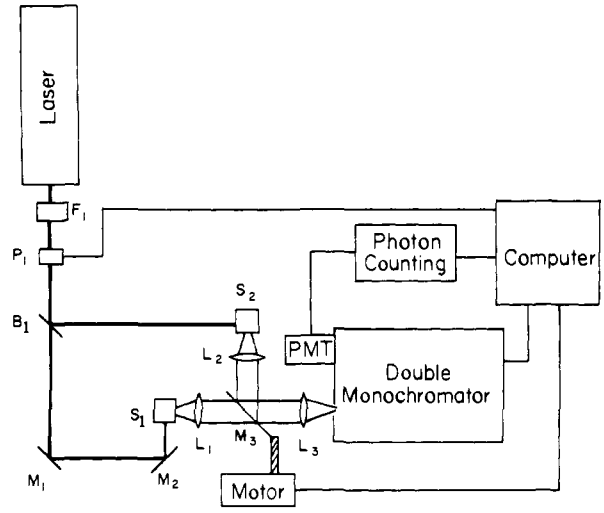

Figure 1. A schematic representation of the Raman difference spectrometer used in this work. Two separate samples, S_1 and S_2, can be studied simultaneously during a single scan of the double monochromator. This eliminates the backlash problems that normally limit accuracy to ±2 cm^{-1} for comparisons between independent scans. The beam splitter, B_1, and mirrors M_1 and M_2 steer and direct the beams to 90° prisms directly underneath the samples. The movable mirror, M_3, is controlled by the computer via a stepping motor. In the "down" position, the light is collected from S_1 via lenses L_1 and L_3; in the "up" position, light is collected from S_2 via lenses L_2 and L_3. Thus, as the monochromator is stepped through the region of interest, two spectra are alternately collected. F_1 is a small quartz premonochromator, and P_1 is a laser-power pick-off, which allows us to correct the spectra for fluctuations in laser power.

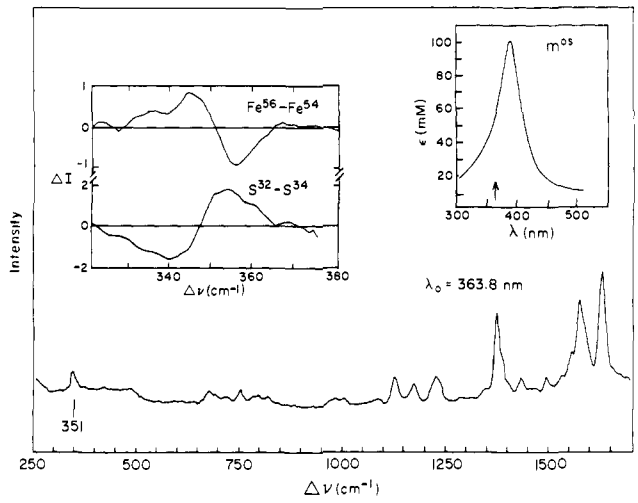

Figure 2. The resonance Raman spectrum of cytochrome $P450_{cam}$ in the ferric camphor-bound state is displayed in the lower curve. The Raman frequencies ($\Delta\nu$) are given with respect to the incident laser energy. The laser wavelength is 363.8 nm in this experiment. The absorption spectrum of the $P450_{cam}$–substrate complex is shown in the upper right-hand corner; the vertical line denotes the position of the resonant laser excitation. The Raman difference spectra in the region of the 351-cm^{-1} Raman mode are displayed in the upper left-hand corner. The vertical scales for the difference spectra are given in units of 1000 counts/channel. The difference spectra presented here are obtained from data that are statistically smoothed by using a nine-point quintic smoothing technique that has been found to have negligible influence on peak positions and band shapes.[25] In addition, linear background contributions to the spectra are substracted before the peak heights (of the 351-cm^{-1} mode) are normalized. A variation in the slope of the background contribution can cause subtle differences in the peak positions. The error limits indicated in the text and in Figure 3 are primarily a reflection of the range of shifts obtained with extreme values of the background slope. The calculation of the isotropic shifts follows the procedure of Laane and Kiefer.[26]

strate specificity vary, all P450 heme proteins are known to catalyze a two-electron-dependent (NADH to NADPH) activation of O_2, yielding hydrocarbon monoxygenation and H_2O release.[2] Molecular characterization of the sequence of catalytic events as well as the structural details of the active site has come primarily from the study of the water-soluble and crystallized bacterial monoxygenase cytochrome $P450_{cam}$, which mediates the stereospecific 5-exo-hydroxylation of the terpene growth substrate D(+)-camphor.[3,4] Thus, the microbial $P450_{cam}$ has offered a useful biological model system for structural and mechanistic study of the entire class of P450 monoxygenases.

The P450 heme proteins were first identified by their unique Soret band position in the ferrous CO complex.[5-7] The structural parameters contributing to this distinct property have since been actively studied by various spectroscopic and chemical probes. The implication of a cysteinyl heme axial ligand was first supported by the similarity of the electron spin resonance spectra of native P450 and metmyoglobin complexed with exogenous thiol ligands.[8-10] A variety of spectroscopic evidence of Fe–S coordination in all of the stable intermediates of the catalytic cycle has since accumulated.[11-15] This evidence includes the significant EXAFS studies,[15] which ultimately rely on spectral comparisons to heme model compounds. Synthetic iron porphyrin complexes with thiolate ligands are most supportive in these assignments,[15-20] particularly as a model for the oxidized high-spin Fe^{3+} enzyme–substrate complex.[19] However, no direct evidence of an Fe–S bond has been presented solely from P450 heme protein studies independent of synthetic compounds.

In this study we employ resonance Raman spectroscopy as a structural probe of the active site of cytochrome $P450_{cam}$. We observe changes in the ground-electronic-state vibrational frequencies, upon isotopic substitution, due to the mass effect. In the present report we discuss results obtained with $P450_{cam}$ samples enriched in ^{34}S (92%) by bacterial culture[21] and in ^{54}Fe (96%) by heme reconstitution of apoprotein.[22] Enriched sulfur was converted to sulfate ($^{34}SO_4^{2-}$) by the Schöniger method and used as the sole, limiting source of sulfur in bacterial growth. Sulfate uptake during culture was monitored with a trace of $^{35}SO_4^{2-}$. Isotope enrichments provided by the Oak Ridge National Laboratory were corrected for known sulfur or iron dilutions during

(2) Sato, R.; Omura, T. "Cytochrome P-450"; Academic Press: New York, 1978.
(3) Gunsalus, I. C.; Meeks, J.; Lipscomb, J.; Debrunner, P.; Munck, E. In "Molecular Mechanisms of Oxygen Activation"; Hayaishi, O., Ed.; Academic Press: New York, 1974; p 559.
(4) Gunsalus, I. C.; Sligar, S. G. *Adv. Enzymol. Relat. Areas Mol. Biol.* **1978**, *47*, 1.
(5) Klingenberg, M. *Arch. Biochem. Biophys.* **1958**, *75*, 376.
(6) Garfinkel, D. *Arch. Biochem. Biophys.* **1958**, *77*, 493.
(7) Omura, T.; Sato, R. *J. Biol. Chem.* **1964**, *239*, 2370.
(8) Murakami, K.; Mason, H. S. *J. Biol. Chem.* **1967**, *242*, 1102.
(9) Jefcoate, C. R. E.; Gaylor, J. L. *Biochemistry* **1969**, *8*, 3464.
(10) Bayer, E.; Hill, H. A. O.; Roder, A.; Williams, R. J. P. *Chem. Commun.* **1969**, *1969*, 109.
(11) Debrunner, P. G.; Gunsalus, I. C.; Sligar, S. G.; Wagner, G. C. In "Metal Ions in Biological Systems"; Sigel, H., Ed.; Marcel Dekker: New York, 1978; p 241.
(12) Gunsalus, I. C.; Wagner, G. C.; Degrunner, P. G. In "Microsomes, Drug Oxidations and Chemical Carcinogenesis"; Coon, M. J., Conney, A., Estabrook, R., Gelboin, J., Gillette, J., O'Brien, R., Eds.; Academic Press: New York, 1980; p 233.
(13) Wagner, G. C.; Gunsalus, I. C.; Wang, M. Y.; Hoffman, B. M. *J. Biol. Chem.* **1981**, *256*, 6266.
(14) LoBrutto, R.; Scholes, C. P.; Wagner, G. C.; Gunsalus, I. C.; Debrunner, P. G. *J. Am. Chem. Soc.* **1980**, *102*, 1167.
(15) Cramer, S. P.; Dawson, J. H.; Hodgson, K.; Hager, L. P. *J. Am. Chem. Soc.* **1978**, *100*, 7282.
(16) Stern, J. O.; Peisach, J. *J. Biol. Chem.* **1974**, *249*, 7495.
(17) Collman, J. P.; Sorrell, T. N. *J. Am. Chem. Soc.* **1975**, *97*, 5948.
(18) Chang, C. K.; Dolphin, D. *J. Am. Chem. Soc.* **1975**, *97*, 5948.
(19) Tang, S. C.; Koch, S.; Papaefthymiou, G. C.; Foner, S.; Frankel, R. B.; Ibers, J. A.; Holm, R. H. *J. Am. Chem. Soc.* **1976**, *98*, 2414.
(20) Caron, C.; Mitschler, A.; Ricard, G. R. L.; Schappacher, M.; Weiss, R. *J. Am. Chem. Soc.* **1979**, *101*, 7401.
(21) Gunsalus, I. C.; Wagner, G. C. *Methods Enzymol.* **1978**, *52*, 166.
(22) Wagner, G. C.; Perez, M.; Toscano, W. A.; Gunsalus, I. C. *J. Biol. Chem.* **1981**, *256*, 6262.

protein preparations. The spectra of the enriched samples are compared directly to the spectra of native protein with nuclei of natural abundance (^{32}S and ^{56}Fe).

The Raman spectrometer used in these experiments is equipped with a computer-controlled double monochromator and a photon counting detection system. The optics of the spectrometer also incorporate a computer-controlled mirror to allow the simultaneous acquisition of Raman spectra from two separate samples (see Figure 1); this allows us to quantitate very small differences in the peak positions of the isotopically labeled samples. A single laser excitation source (λ = 363.8 nm) is employed in the work presented here, although a variety of additional experiments have been performed at other excitation wavelengths and with other isotopic labels. These experiments along with the experimental details will be presented in a future publication.[23] Here we outline some of the recent developments and present unambiguous evidence of the Fe–S bond in the P450 system.

In Figure 2 we present the Raman spectrum of the oxidized enzyme–substrate complex obtained with 363.8-nm excitation (see Champion et al.[24] for a more detailed presentation of the P450$_{cam}$ Raman spectra). The insert at upper right is the absorption spectrum of this complex in the Soret region; the vertical line denotes the position of the laser excitation. The Raman difference spectra (^{32}S – ^{34}S and ^{56}Fe – ^{54}Fe) in the region near 350 cm^{-1} are displayed in the upper left of Figure 2. The derivative shapes of the difference spectra are used to calculate the absolute Raman shifts by the method of Laane and Kiefer.[26] (A small correction is made by computer simulation to account for the less than 100% isotope enrichment.) We find a -4.9 ± 0.3 cm^{-1} downshift in the case of the ^{34}S isotopic substitution and a $+2.5 \pm 0.2$ cm^{-1} upshift in the case of the ^{54}Fe substitution. The results of these two experiments unambiguously demonstrate the existence of an Fe–S linkage in the oxidized enzyme–substrate complex of cytochrome P450$_{cam}$. Moreover, the 351-cm^{-1} mode is assigned to the (predominantly) Fe–S stretching vibration, confirming an earlier suggestion.[27]

It is illustrative at this point to consider the above experiments within a simple normal-mode model consisting of (nuclear) masses connected by springs (the electron bonds). Due to the fact that we have data from two separate experiments that involve both the iron and sulfur masses, the problem is experimentally overdetermined. For example, if we take a simple two-body oscillator model, we have

$$\omega^*/\omega = (\mu/\mu^*)^{1/2} \tag{1}$$

where ω (ω^*) denotes the vibrational frequency of the unlabeled (labeled) oscillator and μ (μ^*) is the reduced mass calculated by using the unlabeled (labeled) masses of iron (m_{Fe}) and sulfur (m_S):

$$\mu = (m_{Fe}m_S)/(m_{Fe} + m_S) \tag{2}$$

The calculated shifts ($\Delta = \omega^* - \omega$) in the two-body model are independent of the force constant between the masses and are found to be $\Delta_{Fe} = +2.4$ cm^{-1} and $\Delta_S = -6.7$ cm^{-1}. The results of the ^{54}Fe/^{56}Fe experiment are well accounted for within this model; however, the ^{34}S/^{32}S experiment shows a significantly smaller shift than predicted. The failure of this simple calculation leads us to consider a somewhat more refined and physically reasonable model.

One obvious extension involves coupling the sulfur atom to both a carbon atom (with force constant k_2) and an iron atom (force constant k_1). We can then utilize the general solution to the three-body oscillator problem that has been discussed by Cross and Van Vleck[28] and by Wilson.[29] If we make the standard

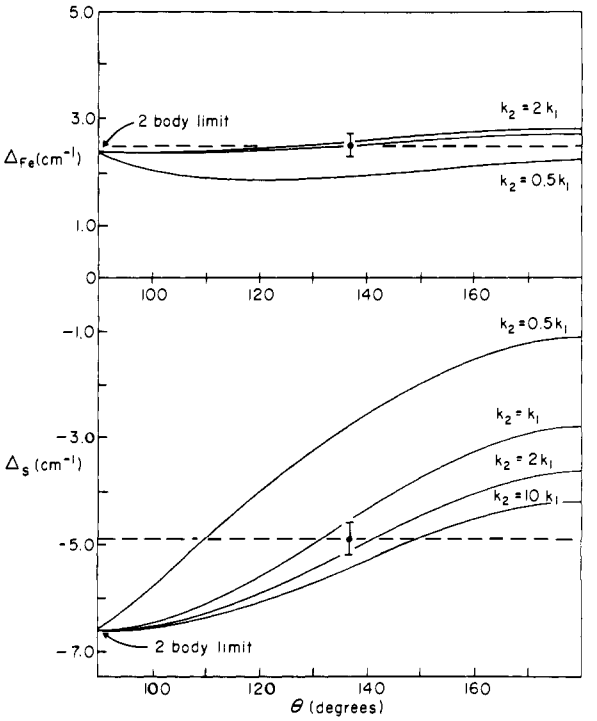

Figure 3. Theoretical predictions of the ^{54}Fe – ^{56}Fe (Δ_{Fe}) and ^{34}S – ^{32}S (Δ_S) Raman shifts by using the three-body oscillator model discussed in the text. Only the results for the low-frequency (351 cm^{-1}) mode are plotted. When the Fe–S–C bond angle, θ, is 90°, the simple two-body result emerges since the Fe–S and C–S modes are orthogonal in this limit. A family of theoretical curves is given in order to show how the Fe–S and C–S force constants (k_1 and k_2, respectively) affect the calculations. Note that the curves describing the variation of Δ_{Fe} with angle are quite closely spaced. The $k_2 = k_1$ curve is found just below the $k_2 = 2k_1$ curve; the $k_2 = 10k_1$ curve is just above the $k_2 = 2k_1$ curve but is not shown because of its proximity. The observed shifts are plotted as horizontal dotted lines, and the error limits are shown. The intersection of the dotted lines with both curves of a given (k_1, k_2) set must occur at the same angle in order to account for the experimental observations. This criterion alone rules out the $k_2 = 0.5k_1$ pair. On the other hand, the (k_1, k_2) sets between $k_2 = k_1$ and $k_2 = 2k_1$ are compatible with experiment if θ lies in the range 125°–145°.

assumption that the bending force constant is much smaller than the stretching force constants[30] k_1 and k_2, we can write down the eigenfrequencies for the stretching vibrations as

$$\omega^2 = \tfrac{1}{2}(k_1/\mu_1 + k_2/\mu_2) \pm \tfrac{1}{2}\{(k_1/\mu_1 + k_2/\mu_2)^2 - 4k_1k_2(1/M^2 + F(\theta)/m_S^2)\}^{1/2} \tag{3}$$

where μ_1, k_1 and μ_2, k_2 are the reduced masses and force constants of the iron–sulfur and carbon–sulfur systems, respectively, m_S is the sulfur mass, and the quantity M^2 is given by

$$M^2 = (m_{Fe}m_Cm_S)/(m_{Fe} + m_C + m_S) \tag{4}$$

The function $F(\theta)$ carries the dependence of the eigenfrequencies on the Fe–S–C bond angle, θ, and is given by

$$F(\theta) = 4\cos^2(\theta/2)\sin^2(\theta/2) \tag{5}$$

The plus sign in eq 3 corresponds to the predominantly C–S stretching vibration, and the minus sign corresponds to the predominantly Fe–S stretching vibration that is under investigation here.

In Figure 3 we have plotted the shifts (Δ_{Fe} and Δ_S) of the 351-cm^{-1} mode that are predicted from eq 3 as the bond angle is varied from 90° to 180°. A family of theoretical curves is shown that represents a variation in the ratio of the Fe–S and S–C force

(23) Stallard, B.; Champion, P. M.; Gunsalus, I. C.; Wagner, G. C., in preparation.
(24) Champion, P. M.; Gunsalus, I. C.; Wagner, G. C. *J. Am. Chem. Soc.* **1978**, *100*, 3743.
(25) Savitzky, A.; Golay, M. *Anal. Chem.* **1964**, *36*, 1627.
(26) Laane, J.; Kiefer, W. *J. Chem. Phys.* **1980**, *72*, 5305.
(27) Felton, R.; Yu, N. In "The Porphyrins"; Dolphin, D., Ed.; Academic Press: New York, 1978; Vol. III, p 347.
(28) Cross, P.; Van Vleck, J. *J. Chem. Phys.* **1933**, *1*, 350.
(29) Wilson, E. *J. Chem. Phys.* **1939**, *7*, 1047.
(30) Herzberg, G. "Infrared and Raman Spectra"; Van Nostrand Reinhold: New York, 1945; p 173.

constants (k_1 and k_2, respectively). Normally, we would expect that k_2 is somewhat greater than k_1 since the C–S stretching vibration of cysteine[31] is found at 683 cm^{-1} and the Fe–S stretching vibration[32] is expected near 350 cm^{-1}, as observed in this study (using these frequencies and the reduced masses, a simple calculation gives $k_2 = 1.63k_1$). However, since the bonding strengths in the Fe–S–C system of cytochrome P450 are not yet known with certainty, we have displayed curves showing the extremes $k_2 = 0.5k_1$ and $k_2 = 10k_1$ as well as the more reasonable values $k_2 = k_1$ and $k_2 = 2k_1$. Perhaps the most striking feature of Figure 3 is the strong dependence of Δ_S on the bond angle. The shift Δ_{Fe} is much less sensitive to the angle due to the larger mass of the iron atom as well as its location at the end (not the middle) of the three-body oscillator.

Superimposed on the theoretical curves in Figure 3 are the experimentally observed shifts, shown as horizontal dotted lines with the errors shown explicitly. Clearly the observed shift, Δ_{Fe}, is quite well approximated by this model for any angle $\lesssim 150°$ and for any $k_2 \gtrsim k_1$. The result for the sulfur shift, Δ_S, is much more constraining, however. Inspection of the figure reveals that, for reasonable values of k_1 and k_2, the bond angle is confined to the range 125°–145°. This is significantly larger than the Fe–S–C bond angle of 100.4° reported for a synthetic P450 model complex.[19]

One reason for this discrepancy may be that the synthetic complex is not a perfect analogue of the P450 system. Crystal packing forces or interactions between the phenyl component of the sulfur ligand and the heme of the synthetic complex could account for at least some of the difference in the bond angles. It also seems feasible that steric constraints imposed by the protein could increase the bond angle in the enzyme system. The EPR spectra of P450 heme proteins, characterized by rhombic ligand fields, show a substantially larger rhombic distortion in $P450_{cam}$ (24%)[33] than in the synthetic analogue (15%).[19] Another interesting possibility involves the increased basicity of the alkyl mercaptide ligand in P450 compared to the aryl nitrobenzenethiolate ligand of the synthetic complex. The degree of iron–sulfur π bonding, predicted by IEH calculations,[34] may therefore be quite different in the two systems. An increase in π-bonding capacity of the more basic cysteine ligand would favor orientation of a sulfur p orbital perpendicular to the Fe–S σ bond. This could be achieved through hybridization of the sulfur valence orbitals to sp^2 and $p_\perp$ (rather than sp^3) and would result in a trigonal bonding geometry with an increase of the Fe–S–C bond angle from ca. 109° to ca. 120°. A strong rhombic distortion of the iron d_π orbitals would also result from this geometry.

On the other hand, more elaborate modeling may conceivably result in a reduction of the predicted bond angle. For example, the coupling of the carbon atom to the protein backbone could be considered. This coupling should be weak, however, due to the fact that the carbon–protein bond angle is expected to be close to the tetrahedral angle of 109°. Iron–porphyrin coupling will also play a minimal role in this normal-mode problem since the Fe–S stretching mode is nearly orthogonal to the Fe–N porphyrin bonds. Another interaction that is not included in the present calculation (T. Kitagawa, private communication) involves the carbon–iron and/or carbon–porphyrin nonbonding repulsive interaction that may cause coupling between the bending and stretching modes of the three-body system (this repulsion would also tend to increase the bond angle). Such interactions are usually very short range, and given the ca. 3-Å iron–carbon distance,[19] we would expect that this effect could be considered as a perturbation on the three-body model presented here. Nevertheless, more elaborate models should be considered in order to quantitate the magnitude of such effects. Details of these calculations will be presented elsewhere.[23] Further insight may also be gained by a careful Raman study of the isotopically labeled synthetic complex.[19] The iron–ligand stretching frequencies of the synthetic complex may provide additional information relating to the Fe–S equilibrium bond distance[35] and the Fe–S–C bond angle in the enzyme system.

In closing, we note that resonance Raman Spectra of the substrate-free cytochrome show no evidence of the 351-cm^{-1} mode for excitation throughout the Soret region.[24] Assuming an Fe–S bond is also present in the substrate-free enzyme,[8-11] this observation strongly indicates that a substantial change in the heme–sulfur interaction takes place when the substrate is bound. This change may directly involve the Fe–S charge-transfer transition moment that is responsible for the resonance enhancement of the 351-cm^{-1} Raman mode; when substrate binds, the charge-transfer transition may either shift into the Soret region or else substantially increase its oscillator strength in the Soret region. (Single crystal optical studies have previously revealed a z-polarized charge-transfer state within the Soret band of the $P450_{cam}$ substrate complex.[4,11,34]) The fact that the heme iron atom changes from low spin ($S = {}^1/_2$) to predominantly high spin ($S = {}^5/_2$) upon substrate binding[4,11] is supportive of this observation. Since the iron d_π orbitals of the low-spin form are thought to be filled,[11] we might expect that the substrate-induced spin transition (and concomitant vacancy in the d_π orbitals) acts as a "switch" that controls the sulfur–heme iron π-bonding as well as the charge-transfer properties.

Finally, we note that the resonance enhancement effect, quantitated as the laser excitation is tuned through an absorption band (i.e., measurement of a Raman excitation profile), can offer a great deal of information about both the nature of the excited molecular state(s) and the strength of the electron–nuclear coupling.[36,37] If the laser frequency is such that an iron–sulfur charge-transfer resonance condition is optimized, we expect enhancement of the scattering amplitudes of the iron–sulfur mode. In fact, now that such an iron–sulfur mode is definitely identified (e.g., the 351-cm^{-1} mode), a careful study of its Raman excitation profile will allow us to extract a great deal of information about the shape and absolute intensity of the charge-transfer transition. Recent theoretical developments in this area have shown how the Raman excitation profile and the absorption band shape (and intensity) are related in a general way.[38-40] This opens up the possibility of using the Raman excitation profile of an iron–axial ligand mode to "deconvolute" the iron–ligand charge-transfer band from within a spectrally congested region.

Acknowledgment. P.M.C. acknowledges helpful discussions with L. H. Berka, W. D. Hobey, and S. J. Weininger. This work was supported by grants from the National Institutes of Health (AM00562, GM21161, and AM30714).

(31) Garfinkel, D.; Edsall, J. *J. Am. Chem. Soc.* **1958**, *80*, 3823.
(32) Tang, S.; Spiro, T.; Antanaltis, C.; Holm, R.; Herskovitz, T.; Mortensen, L. *Biochem. Biophys. Res. Commun.* **1975**, *62*, 1.
(33) Tsal, R.; Yu, C-A.; Gunsalus, I. C.; Peisach, J.; Blumberg, W.; Orme-Johnson, W. H.; Beinert, H. *Proc. Natl. Acad. Sci. U.S.A.* **1970**, *66*, 1157.
(34) Hanson, L.; Sligar, S.; Gunsalus, I. C. *Croat. Chem. Acta* **1977**, *49*, 237.
(35) Asher, S.; Schuster, T. *Biochemistry* **1979**, *18*, 5377.
(36) Tang, J.; Albrecht, A. C. In "Raman Spectroscopy"; Szymanski, H., Ed.; Plenum: New York, 1970; p 33.
(37) Champion, P. M.; Albrecht, A. C. *J. Chem. Phys.* **1979**, *71*, 1110; **1980**, *72*, 6498.
(38) Tonks, D. L.; Page, J. *Chem. Phys. Lett.* **1979**, *66*, 449.
(39) Hassing, L.; Mortensen, O. J. *J. Chem. Phys.* **1980**, *73*, 1078.
(40) Champion, P. M.; Albrecht, A. C. *Chem. Phys. Lett.* **1981**, *82*, 410.